

# Multidimensional Resonance Analysis of

$$\Lambda_c^+ \rightarrow pK^-\pi^+$$

E. M. Aitala,<sup>i</sup> S. Amato,<sup>a</sup> J. C. Anjos,<sup>a</sup> J. A. Appel,<sup>e</sup>  
 D. Ashery,<sup>n</sup> S. Banerjee,<sup>e</sup> I. Bediaga,<sup>a</sup> G. Blaylock,<sup>h</sup>  
 S. B. Bracker,<sup>o</sup> P. R. Burchat,<sup>m</sup> R. A. Burnstein,<sup>f</sup> T. Carter,<sup>e</sup>  
 H. S. Carvalho,<sup>a</sup> N. K. Copty,<sup>l</sup> L. M. Cremaldi,<sup>i</sup> C. Darling,<sup>r</sup>  
 K. Denisenko,<sup>e</sup> S. Devmal,<sup>c</sup> A. Fernandez,<sup>k</sup> G. F. Fox,<sup>l</sup>  
 P. Gagnon,<sup>b</sup> C. Gobel,<sup>a</sup> K. Gounder,<sup>i</sup> A. M. Halling,<sup>e</sup>  
 G. Herrera,<sup>d</sup> G. Hurvits,<sup>n</sup> C. James,<sup>e</sup> P. A. Kasper,<sup>f</sup>  
 S. Kwan,<sup>e</sup> D. C. Langs,<sup>l</sup> J. Leslie,<sup>b</sup> B. Lundberg,<sup>e</sup> J. Magnin,<sup>a</sup>  
 S. MayTal-Beck,<sup>n</sup> B. Meadows,<sup>c</sup> J. R. T. de Mello Neto,<sup>a</sup>  
 D. Mihalcea,<sup>g</sup> R. H. Milburn,<sup>p</sup> J. M. de Miranda,<sup>a</sup> A. Napier,<sup>p</sup>  
 A. Nguyen,<sup>g</sup> A. B. d'Oliveira,<sup>c,k</sup> K. O'Shaughnessy,<sup>b</sup>  
 K. C. Peng,<sup>f</sup> L. P. Perera,<sup>c</sup> M. V. Purohit,<sup>l</sup> B. Quinn,<sup>i</sup>  
 S. Radeztsky,<sup>q</sup> A. Rafatian,<sup>i</sup> N. W. Reay,<sup>g</sup> J. J. Reidy,<sup>i</sup>  
 A. C. dos Reis,<sup>a</sup> H. A. Rubin,<sup>f</sup> D. A. Sanders,<sup>i</sup>  
 A. K. S. Santha,<sup>c</sup> A. F. S. Santoro,<sup>a</sup> A. J. Schwartz,<sup>c</sup>  
 M. Sheaff,<sup>d,q</sup> R. A. Sidwell,<sup>g</sup> A. J. Slaughter,<sup>r</sup> M. D. Sokoloff,<sup>c</sup>  
 J. Solano,<sup>a</sup> N. R. Stanton,<sup>g</sup> R. J. Stefanski,<sup>e</sup> K. Stenson,<sup>q</sup>  
 D. J. Summers,<sup>i</sup> S. Takach,<sup>r</sup> K. Thorne,<sup>e</sup> A. K. Tripathi,<sup>g</sup>  
 S. Watanabe,<sup>q</sup> R. Weiss-Babai,<sup>n</sup> J. Wiener,<sup>j</sup> N. Witchey,<sup>g</sup>  
 E. Wolin,<sup>r</sup> S. M. Yang,<sup>g</sup> D. Yi,<sup>i</sup> S. Yoshida,<sup>g</sup> R. Zaliznyak,<sup>m</sup>  
 C. Zhang,<sup>g</sup>

## Fermilab E791 Collaboration

<sup>a</sup>*Centro Brasileiro de Pesquisas Físicas, Rio de Janeiro RJ, Brazil*

<sup>b</sup>*University of California, Santa Cruz, California 95064*

<sup>c</sup>*University of Cincinnati, Cincinnati, Ohio 45221*

<sup>d</sup>*CINVESTAV, 07000 Mexico City, DF Mexico*

<sup>e</sup>*Fermilab, Batavia, Illinois 60510*

<sup>f</sup>*Illinois Institute of Technology, Chicago, Illinois 60616*

<sup>g</sup>*Kansas State University, Manhattan, Kansas 66506*

<sup>h</sup>*University of Massachusetts, Amherst, Massachusetts 01003*

<sup>i</sup>*University of Mississippi-Oxford, University, Mississippi 38677*

<sup>j</sup>*Princeton University, Princeton, New Jersey 08544*

<sup>k</sup>*Universidad Autonoma de Puebla, Puebla, Mexico*

<sup>l</sup>*University of South Carolina, Columbia, South Carolina 29208*

<sup>m</sup>*Stanford University, Stanford, California 94305*

<sup>n</sup>*Tel Aviv University, Tel Aviv, 69978 Israel*

<sup>o</sup>*Box 1290, Enderby, British Columbia, V0E 1V0, Canada*

<sup>p</sup>*Tufts University, Medford, Massachusetts 02155*

<sup>q</sup>*University of Wisconsin, Madison, Wisconsin 53706*

<sup>r</sup>*Yale University, New Haven, Connecticut 06511*

---

## Abstract

We present the results of a five-dimensional resonant amplitude analysis of the  $\Lambda_c^+ \rightarrow pK^- \pi^+$  system based on  $946 \pm 38$  reconstructed decays. These data were produced in 500 GeV/c  $\pi^-$ -N interactions by Fermilab experiment E791. We report measurements of the amplitudes for  $\Lambda_c^+$  decay into nonresonant  $pK^- \pi^+$  and to  $p\bar{K}^{*0}(890)$ ,  $\Delta^{++}(1232)K^-$ , and  $\Lambda(1520)\pi^+$  and we comment on other possible resonant enhancements. This is the first complete amplitude analysis of the  $\Lambda_c^+ \rightarrow pK^- \pi^+$  system. We find that  $(54.8 \pm 5.5 \pm 3.5)\%$  of the decays are nonresonant,  $(19.5 \pm 2.6 \pm 1.8)\%$  of the decays are via the  $\bar{K}^{*0}$  resonance,  $(18.0 \pm 2.9 \pm 2.9)\%$  of the decays are via the  $\Delta^{++}$  resonance, and  $(7.7 \pm 1.8 \pm 1.1)\%$  of the decays are via the  $\Lambda(1520)$  resonance. We find evidence for an increasingly negative polarization of the  $\Lambda_c^+$  baryons as a function of  $p_T^2$ , in agreement with a recent model[1] and with a related measurement[2].

*Key words:* Multidimensional, Resonance,  $\Lambda_c$ , Polarization

*PACS:* 13.30 a,13.30.Eg,13.88.+e,14.20.Lq

---

## 1 Introduction

Since the discovery of charm in 1974, great progress has been made in the understanding of charm meson decays. Charm meson lifetimes, branching fractions, and resonant decays have been studied extensively[3]. While charm baryon lifetimes and branching fractions have also been measured, these measurements are not as complete, and no information is available on the amplitude analysis of any charm baryon decay system. Measurements of charm baryon decays yield information regarding the relative importance of spectator and exchange amplitudes. The latter are thought to play a leading role

in enhancing charm baryon decay rates. The most obvious components of the  $\Lambda_c^+ \rightarrow pK^-\pi^+$  decays (and charge conjugate decays, which are implied throughout this paper) include the nonresonant  $pK^-\pi^+$  decay as well as the  $p\bar{K}^{*0}(890)$  and  $\Lambda(1520)\pi^+$  two-body decays. All three of these decays can be described by spectator and W-exchange amplitudes. In lowest order, the  $\Delta^{++}(1232)K^-$  decay can occur only via the exchange amplitude. Exchange amplitudes are suppressed in charm meson decays, at least at the quark level, because of helicity and form-factor effects. These effects are not expected to inhibit exchange amplitudes for charm baryons due to the three-body nature of the interaction. To understand fully this system of decays, as well as other charmed baryon decays, a complete resonant amplitude analysis is needed.

The charm baryon and its decay products carry spin and the charm baryon may be polarized upon production. Previous charm pseudoscalar meson decay analyses have studied structure in the two-dimensional space of the decay product effective masses (Dalitz plot distributions), but the spin effects just described require five kinematic variables for a complete description. While this complicates the analysis, it affords greater sensitivity to the parameters of interest. As a by-product of the analysis, the production polarization of the  $\Lambda_c^+$ ,  $\mathbf{P}_{\Lambda_c}$ , is also measured. This analysis is the first five-dimensional amplitude analysis and, as such, is unique.

## 2 Formalism

We parameterize the observed decay rate as a function of the  $\Lambda_c^+$  polarization,  $\mathbf{P}_{\Lambda_c}$ , and of the magnitudes and relative phases of each intermediate two-body resonance decay amplitude. We assume that the nonresonant decay is described by an amplitude that is constant across phase space. The differential decay rate  $d\Gamma$  (or signal density  $S$ ) may be expressed as

$$d\Gamma \sim S(\vec{x}) = \frac{(1 + \mathbf{P}_{\Lambda_c})}{2} (|\sum_{\mathbf{r}} B_{\mathbf{r}}(m_{\mathbf{r}})\alpha_{\mathbf{r},\frac{1}{2},\frac{1}{2}}|^2 + |\sum_{\mathbf{r}} B_{\mathbf{r}}(m_{\mathbf{r}})\alpha_{\mathbf{r},\frac{1}{2},-\frac{1}{2}}|^2) + \frac{(1 - \mathbf{P}_{\Lambda_c})}{2} (|\sum_{\mathbf{r}} B_{\mathbf{r}}(m_{\mathbf{r}})\alpha_{\mathbf{r},-\frac{1}{2},\frac{1}{2}}|^2 + |\sum_{\mathbf{r}} B_{\mathbf{r}}(m_{\mathbf{r}})\alpha_{\mathbf{r},-\frac{1}{2},-\frac{1}{2}}|^2) \quad (1)$$

where  $\alpha_{\mathbf{r},m,\lambda_p}$  is the complex decay amplitude for resonance  $\mathbf{r}$  given  $m$ , the spin projection of the  $\Lambda_c$  on the  $z$ -axis, and  $\lambda_p$ , the proton helicity in the  $\Lambda_c$  rest frame.

$B_{\mathbf{r}}(m_{\mathbf{r}})$  in Equation 1 is the normalized relativistic Breit-Wigner amplitude

corrected for the centrifugal barrier[4]. Given the decay mode  $\Lambda_c \rightarrow r(\rightarrow ab)c$ ,

$$B_r(m_r) = (-2|p_c||p_a|)^L \frac{F_{\Lambda_c} F_r}{m_0^2 - m_r^2 - im_0 \Gamma_r} \quad (2)$$

where

$$\Gamma_r = \Gamma_0 \left(\frac{q}{q_0}\right)^{2L+1} \frac{m_0}{m_r} \frac{F_r^2(q)}{F_r^2(q_0)} \quad (3)$$

for resonance  $r$  of angular momentum  $L$  at the reconstructed two body mass  $m_r$  with the momentum  $q$  (and  $q_0$  when  $m_r = m_0$ ) of a daughter particle in the resonance's rest frame, and with resonance mass and width  $m_0$  and  $\Gamma_0$  as found in Ref. [3]. Using this convention, we set  $B_r(m_r)$  for the nonresonant decay to be 1.  $F_L$  is the strong coupling factor at the appropriate decay vertex, and takes the Blatt-Weisskopf form as described in Table 1. Table 2 lists the range of the strong interaction,  $R_X$ .

Table 1

The expressions for  $F$  used in the Breit-Wigner amplitude.

$L$	$F_L$
0	1
1	$(1 + R_X^2 q^2)^{-1/2}$
2	$(9 + 3R_X^2 q^2 + R_X^4 q^4)^{-1/2}$

Table 2

The values of  $R$  used in the Breit-Wigner amplitude.

$X$	$R_X$ $(\text{GeV}/c^2)^{-1}$
$\bar{K}^{*0}(890)$	3.4 [5]
$\Delta^{++}(1232)$	5.22 [6]
$\Lambda(1520)$	6.29 [7]
$\Lambda_c^+$	5.07 [8]

In Tables 3–6, where the amplitudes  $\alpha_{r,m,\lambda_p}$  (derived using the helicity formalism described in Ref. [9]) can be seen more explicitly, the direction  $(\phi_r, \theta_r)$  is the direction of the resonance,  $r$ , in the  $\Lambda_c$  rest frame, using the convention

of Ref. [10]. The primed angles refer to the direction of one of the resonance's daughters in the resonance's rest frame. Note that the decay amplitudes for each resonance may have contributions to each of the four terms in Equation 1.

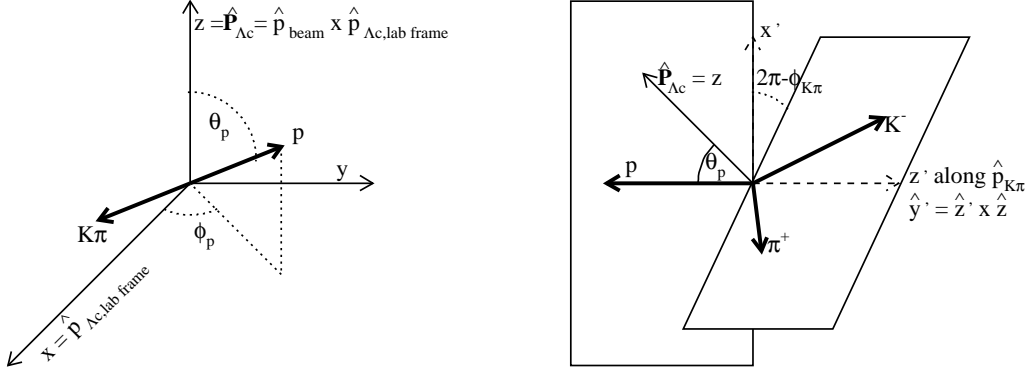


Fig. 1. Definition of angles using  $\Lambda_c^+ \rightarrow p\bar{K}^{*0} \rightarrow pK^-\pi^+$  as an example. In both figures the  $\Lambda_c^+$  is at rest. In the first figure, which defines  $(\theta_p, \phi_p)$ , the  $x$ -axis is along the direction of motion of the  $\Lambda_c^+$  in the lab frame and the  $z$ -axis is the polarization axis, normal to the plane of production. In the second figure we define  $\phi_{K\pi}$  as the angle between the plane containing the  $\bar{K}^{*0}$  decay products and the plane containing the proton and the  $x$ -axis.

Each event in the final data sample is described by five kinematic variables of interest (two two-body masses and the decay angles  $\theta_p$ ,  $\phi_p$ , and  $\phi_{K\pi}$  as defined in Figure 1) which are determined after the  $pK\pi$  reconstructed mass is constrained to the  $\Lambda_c$  mass. We chose the quantization axis (the  $z$ -axis in the  $\Lambda_c$  rest frame) to be normal to the  $\Lambda_c$  production plane (as defined by  $\hat{p}_{\text{beam}} \times \hat{p}_{\Lambda_c}$ , where  $\hat{p}_{\text{beam}}$  is the beam direction and  $\hat{p}_{\Lambda_c}$  is the  $\Lambda_c$  production direction in the lab frame). The  $x$ -axis in the  $\Lambda_c$  rest frame is chosen to be the direction of the  $\Lambda_c$  in the lab frame.

### 3 Experiment E791 and Data Selection

We analyze data from Fermilab fixed-target experiment E791, which ran during 1991 and 1992. The data were recorded from 500 GeV/ $c$   $\pi^-$  beam interactions in five thin target foils (one platinum, four diamond) whose centers were separated by about 1.53 cm. The detector, described elsewhere in more detail[11,12], was a large-acceptance, forward, two-magnet spectrometer. The key components for this study were eight planes of multiwire proportional chambers, and six planes of silicon microstrip detectors (SMD) before the target for beam tracking, a 17-plane SMD system and 35 drift chamber planes downstream of the target for track and vertex reconstruction, and two multi-cell threshold Čerenkov counters for charged particle identification.

Table 3

Amplitudes for the  $\Lambda_c^+(\frac{1}{2}^+) \rightarrow (\overline{K}^{*0}(890)(1^-) \rightarrow K^-\pi^+)p(\frac{1}{2}^+)$  decay mode.

m	$\lambda_p$	Amplitude
$\frac{1}{2}$	$\frac{1}{2}$	$E_1 e^{i\phi_{E_1}} d_{\frac{1}{2}\frac{1}{2}}^{\frac{1}{2}}(\theta_{\overline{K}^{*0}}) d_{10}^1(\theta'_K) e^{i\phi'_K} + E_2 e^{i\phi_{E_2}} d_{\frac{1}{2}-\frac{1}{2}}^{\frac{1}{2}}(\theta_{\overline{K}^{*0}}) d_{00}^1(\theta'_K) e^{i\phi_{\overline{K}^{*0}}}$
$\frac{1}{2}$	$-\frac{1}{2}$	$E_3 e^{i\phi_{E_3}} d_{\frac{1}{2}\frac{1}{2}}^{\frac{1}{2}}(\theta_{\overline{K}^{*0}}) d_{00}^1(\theta'_K) + E_4 e^{i\phi_{E_4}} d_{\frac{1}{2}-\frac{1}{2}}^{\frac{1}{2}}(\theta_{\overline{K}^{*0}}) d_{-10}^1(\theta'_K) e^{i(\phi_{\overline{K}^{*0}} - \phi'_K)}$
$-\frac{1}{2}$	$\frac{1}{2}$	$E_1 e^{i\phi_{E_1}} d_{-\frac{1}{2}\frac{1}{2}}^{\frac{1}{2}}(\theta_{\overline{K}^{*0}}) d_{10}^1(\theta'_K) e^{-i(\phi_{\overline{K}^{*0}} - \phi'_K)} + E_2 e^{i\phi_{E_2}} d_{-\frac{1}{2}-\frac{1}{2}}^{\frac{1}{2}}(\theta_{\overline{K}^{*0}}) d_{00}^1(\theta'_K)$
$-\frac{1}{2}$	$-\frac{1}{2}$	$E_3 e^{i\phi_{E_3}} d_{-\frac{1}{2}\frac{1}{2}}^{\frac{1}{2}}(\theta_{\overline{K}^{*0}}) d_{00}^1(\theta'_K) e^{-i\phi_{\overline{K}^{*0}}} + E_4 e^{i\phi_{E_4}} d_{-\frac{1}{2}-\frac{1}{2}}^{\frac{1}{2}}(\theta_{\overline{K}^{*0}}) d_{-10}^1(\theta'_K) e^{-i\phi'_K}$

Table 4

Amplitudes for the  $\Lambda_c^+(\frac{1}{2}^+) \rightarrow (\Delta^{++}(1232)(\frac{3}{2}^+) \rightarrow p\pi^+)K^-$  decay mode.

m	$\lambda_p$	Amplitude
$\frac{1}{2}$	$\frac{1}{2}$	$F_1 e^{i\phi_{F_1}} d_{\frac{1}{2}\frac{1}{2}}^{\frac{1}{2}}(\theta_{\Delta^{++}}) d_{\frac{3}{2}\frac{1}{2}}^{\frac{3}{2}}(\theta'_p) + F_2 e^{i\phi_{F_2}} d_{\frac{1}{2}-\frac{1}{2}}^{\frac{1}{2}}(\theta_{\Delta^{++}}) d_{-\frac{3}{2}\frac{1}{2}}^{\frac{3}{2}}(\theta'_p) e^{i(\phi_{\Delta^{++}} - \phi'_p)}$
$\frac{1}{2}$	$-\frac{1}{2}$	$F_1 e^{i\phi_{F_1}} d_{\frac{1}{2}\frac{1}{2}}^{\frac{1}{2}}(\theta_{\Delta^{++}}) d_{\frac{3}{2}-\frac{1}{2}}^{\frac{3}{2}}(\theta'_p) e^{i\phi'_p} + F_2 e^{i\phi_{F_2}} d_{\frac{1}{2}-\frac{1}{2}}^{\frac{1}{2}}(\theta_{\Delta^{++}}) d_{-\frac{3}{2}-\frac{1}{2}}^{\frac{3}{2}}(\theta'_p) e^{i\phi_{\Delta^{++}}}$
$-\frac{1}{2}$	$\frac{1}{2}$	$F_1 e^{i\phi_{F_1}} d_{-\frac{1}{2}\frac{1}{2}}^{\frac{1}{2}}(\theta_{\Delta^{++}}) d_{\frac{3}{2}\frac{1}{2}}^{\frac{3}{2}}(\theta'_p) e^{-i\phi_{\Delta^{++}}} + F_2 e^{i\phi_{F_2}} d_{-\frac{1}{2}-\frac{1}{2}}^{\frac{1}{2}}(\theta_{\Delta^{++}}) d_{-\frac{3}{2}\frac{1}{2}}^{\frac{3}{2}}(\theta'_p) e^{-i\phi'_p}$
$-\frac{1}{2}$	$-\frac{1}{2}$	$F_1 e^{i\phi_{F_1}} d_{-\frac{1}{2}\frac{1}{2}}^{\frac{1}{2}}(\theta_{\Delta^{++}}) d_{\frac{3}{2}-\frac{1}{2}}^{\frac{3}{2}}(\theta'_p) e^{-i(\phi_{\Delta^{++}} - \phi'_p)} + F_2 e^{i\phi_{F_2}} d_{-\frac{1}{2}-\frac{1}{2}}^{\frac{1}{2}}(\theta_{\Delta^{++}}) d_{-\frac{3}{2}-\frac{1}{2}}^{\frac{3}{2}}(\theta'_p)$

An unrestrictive, open-charm event selection based on total transverse energy seen in the calorimeters was made in real time. Offline we require all  $\Lambda_c$  event candidates to have a production and decay vertex longitudinally separated by at least  $6\sigma_1$ , where  $\sigma_1$  is the error in that separation. The tracks and vertex fits satisfy  $\chi^2$  requirements. The vertex must be formed from proton, kaon, and pion tracks identified as such by the Čerenkov particle identification system. Proton candidates are rejected when projected into regions of the detector with poor particle identification efficiency. To reject more background, we require that the magnitude of the vector sum of the transverse momenta of all the secondary tracks with respect to the flight path of the reconstructed

Table 5

Amplitudes for the  $\Lambda_c^+(\frac{1}{2}^+) \rightarrow (\Lambda(1520))(\frac{3}{2}^-) \rightarrow pK^-\pi^+$  decay mode.

m	$\lambda_p$	Amplitude
$\frac{1}{2}$	$\frac{1}{2}$	$H_1 e^{i\phi_{H_1}} d_{\frac{1}{2}\frac{1}{2}}^{\frac{1}{2}}(\theta_{\Lambda(1520)}) d_{\frac{1}{2}\frac{1}{2}}^{\frac{3}{2}}(\theta'_p) + H_2 e^{i\phi_{H_2}} d_{\frac{1}{2}-\frac{1}{2}}^{\frac{1}{2}}(\theta_{\Lambda(1520)}) d_{-\frac{1}{2}\frac{1}{2}}^{\frac{3}{2}}(\theta'_p) e^{i(\phi_{\Lambda(1520)} - \phi'_p)}$
$\frac{1}{2}$	$-\frac{1}{2}$	$-(H_1 e^{i\phi_{H_1}} d_{\frac{1}{2}\frac{1}{2}}^{\frac{1}{2}}(\theta_{\Lambda(1520)}) d_{\frac{1}{2}-\frac{1}{2}}^{\frac{3}{2}}(\theta'_p) e^{i\phi'_p} + H_2 e^{i\phi_{H_2}} d_{\frac{1}{2}-\frac{1}{2}}^{\frac{1}{2}}(\theta_{\Lambda(1520)}) d_{-\frac{1}{2}-\frac{1}{2}}^{\frac{3}{2}}(\theta'_p) e^{i\phi_{\Lambda(1520)}})$
$-\frac{1}{2}$	$\frac{1}{2}$	$H_1 e^{i\phi_{H_1}} d_{-\frac{1}{2}\frac{1}{2}}^{\frac{1}{2}}(\theta_{\Lambda(1520)}) d_{\frac{1}{2}\frac{1}{2}}^{\frac{3}{2}}(\theta'_p) e^{-i\phi_{\Lambda(1520)}} + H_2 e^{i\phi_{H_2}} d_{-\frac{1}{2}-\frac{1}{2}}^{\frac{1}{2}}(\theta_{\Lambda(1520)}) d_{-\frac{1}{2}\frac{1}{2}}^{\frac{3}{2}}(\theta'_p) e^{-i\phi'_p}$
$-\frac{1}{2}$	$-\frac{1}{2}$	$-(H_1 e^{i\phi_{H_1}} d_{-\frac{1}{2}\frac{1}{2}}^{\frac{1}{2}}(\theta_{\Lambda(1520)}) d_{\frac{1}{2}-\frac{1}{2}}^{\frac{3}{2}}(\theta'_p) e^{-i(\phi_{\Lambda(1520)} - \phi'_p)} + H_2 e^{i\phi_{H_2}} d_{-\frac{1}{2}-\frac{1}{2}}^{\frac{1}{2}}(\theta_{\Lambda(1520)}) d_{-\frac{1}{2}-\frac{1}{2}}^{\frac{3}{2}}(\theta'_p))$

Table 6

Amplitudes for the nonresonant  $\Lambda_c^+(\frac{1}{2}^+) \rightarrow pK^-\pi^+$  decay mode.

m	$\lambda_p$	Amplitude
$\frac{1}{2}$	$\frac{1}{2}$	$N_{++} e^{i\phi_{N_{++}}}$
$\frac{1}{2}$	$-\frac{1}{2}$	$N_{+-} e^{i\phi_{N_{+-}}}$
$-\frac{1}{2}$	$\frac{1}{2}$	$N_{-+} e^{i\phi_{N_{-+}}}$
$-\frac{1}{2}$	$-\frac{1}{2}$	$N_{--} e^{i\phi_{N_{--}}}$

$\Lambda_c$  candidate be  $\leq 0.4$  GeV/ $c$ . To eliminate reflections from  $D^+ \rightarrow K^-\pi^+\pi^+$  decays and from  $D^+$ ,  $D_s^+ \rightarrow K^-K^+\pi^+$  decays, we remove all events whose reconstructed  $K\pi\pi$  mass is within the range [1.85, 1.89] GeV/ $c^2$  or whose reconstructed  $KK\pi$  mass is within the ranges [1.85, 1.89] GeV/ $c^2$  or [1.95, 1.99] GeV/ $c^2$ .

After this preliminary stage of the analysis, we have  $998 \pm 167$   $\Lambda_c^+ \rightarrow pK^-\pi^+$  signal events and  $107\,368 \pm 366$  background events. Therefore we apply further requirements in order to improve this signal in an unbiased way. This is ac-

completed by a selection on the output of an artificial neural network. The network is trained using a Monte Carlo (MC) sample of  $\Lambda_c^+ \rightarrow pK^-\pi^+$  decays for signal and events from the wings of the  $pK^-\pi^+$  mass distribution in data for background. The variables used in the training include all those described in the preliminary analysis above and the transverse miss distance between the primary vertex and the line of flight of the reconstructed  $\Lambda_c$  candidate, the scalar sum of the  $p_T^2$  of all the secondary tracks with respect to the flight path of the reconstructed  $\Lambda_c$  candidate, the significance of the separation between the secondary vertex and the closest target foil edge, the calculated proper lifetime of the reconstructed  $\Lambda_c$ , the ratio of the distance of each of the decay tracks from the secondary vertex to its distance from the primary vertex, and the minimum and product of the three ratios.

The cut on the neural net output is chosen to maximize  $N_{S,MC}/\sqrt{N_{S,MC} + N_B}$  where  $N_{S,MC}$  is the number of MC signal events (scaled to our data size) and  $N_B$  the number of background events in the signal region. After the cut on the neural net output, 2271 real events in the  $pK^-\pi^+$  mass range of [2.18, 2.38]  $\text{GeV}/c^2$  survive, as seen in Figure 2.

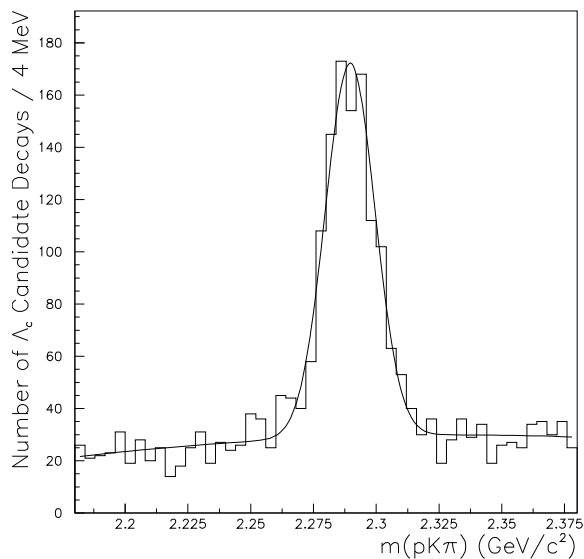


Fig. 2.  $\Lambda_c \rightarrow pK\pi$  signal used in this analysis.

#### 4 Differential Decay Rate Fit

Once the final data set is established we constrain each reconstructed  $pK\pi$  mass to the mass of the  $\Lambda_c$ . This forces all candidate events, whether in the signal peak or in the wings, to have the same decay phase space as that of the signal. We describe each event by the five independent kinematic variables of interest ( $m^2(K\pi)$ ,  $m^2(p\pi)$ ,  $\cos(\theta_p)$ ,  $\phi_p$ , and  $\phi_{K\pi}$ ).



Next we use an extended maximum likelihood technique to fit the data. The likelihood is assumed to have the form

$$\ln \mathcal{L} = \sum_i \ln \mathcal{L}_i - \left( \frac{1}{2} \ln [2\pi N_{\text{pred}}] + \frac{[N_{\text{pred}} - N_{\text{obs}}]^2}{2N_{\text{pred}}} \right), \quad (4)$$

where  $N_{\text{pred}} = N_S + N_B$  and  $N_{\text{obs}}$  are the predicted and observed numbers of events, and  $\mathcal{L}_i$  is the likelihood of each event defined by a joint probability density in the five-dimensional phase space of the decay and the one-dimensional space of unconstrained  $m_{pK\pi}$  (Fig. 2).

The likelihood for an individual event is given by

$$\mathcal{L}_i = \frac{N_S}{N_S + N_B} G(m_{pK\pi,i}, x_F) S(\vec{x}_i) A(\vec{x}_i) + \frac{N_B}{N_S + N_B} Q(m_{pK\pi,i}) B(\vec{x}_i) \quad (5)$$

Here  $G$  and  $Q$  represent normalized Gaussian and quadratic functions of the three body mass  $m_{pK\pi}$  while  $S(\vec{x})$ ,  $A(\vec{x})$ , and  $B(\vec{x})$  are the signal, acceptance, and background normalized densities in the five-dimensional space of decay kinematic variables described previously. Note that the width of  $G$  is dependent on  $x_F$ , the scaled longitudinal momentum of the  $\Lambda_c$ -candidate, and is parameterized as  $\sigma = \sigma_a \times x_F + \sigma_b$ . Our  $x_F$  range is essentially  $[-0.1, +0.4]$ . The function  $S(\vec{x})$  is described in Equation 1, while  $A(\vec{x})$  is a model of the acceptance, a five-dimensional density of the reconstructed and surviving uniformly-generated MC events, and  $B(\vec{x})$  is a model of the background, coming from a five-dimensional density of data events in the wings of the mass plot. We model our acceptance,  $A(\vec{x})$ , and background,  $B(\vec{x})$ , using the same approach. This common procedure is based on the  $K$ -nearest-neighbors method[13]. The  $K$ -nearest-neighbors method works on the principle that the density at a point in phase space is proportional to  $N/V(r(\vec{x}_i))$  where  $N$  is the number of events which occur within volume  $V(r(\vec{x}_i))$  which is a multidimensional sphere of radius  $r$  centered at  $\vec{x}_i$ . This method is augmented to ensure that each of the one-dimensional projections of the five-dimensional density in question ( $A(\vec{x})$  and  $B(\vec{x})$ ) matches the corresponding projection of the data set modeled (accepted MC events and background events from the data wings, respectively).

Using the fitting software, MINUIT[14], we find the parameter values which maximize  $\mathcal{L}$  in Equation 4. The results can be seen in Table 7. Because the polarization is dependent on transverse momentum[1], we split the data set into three equally populated regions of  $p_T^2$  (0.00–0.70 GeV/c, 0.70–1.24 GeV/c, and 1.24–5.20 GeV/c) and find the polarization for each region ( $\mathbf{P}_{\Lambda_c,1}$ ,  $\mathbf{P}_{\Lambda_c,2}$ , and  $\mathbf{P}_{\Lambda_c,3}$ , respectively). The polarization versus  $p_T^2$  is shown in Figure 3.

Figure 4 shows the one-dimensional projections of the overall fit using the parameters of Table 7 and the data in the signal region. The  $\chi^2/\text{DOF}$  for the

Table 7

Decay amplitudes, polarization, and mass plot parameters for  $\Lambda_c \rightarrow pK\pi$  from the MINUIT fit with statistical errors. The two parameters without errors are the only ones that are fixed.

Terms	Parameter	Value
$p\overline{K}^{*0}(890)$	$E_1$	$0.52 \pm 0.17$
	$\phi_{E_1}$	$-1.01 \pm 0.48$
	$E_2$	$0.20 \pm 0.10$
	$\phi_{E_2}$	$2.35 \pm 0.67$
	$E_3$	$0.21 \pm 0.10$
	$\phi_{E_3}$	$3.46 \pm 0.42$
	$E_4$	$0.16 \pm 0.10$
	$\phi_{E_4}$	$5.29 \pm 0.55$
$\Delta^{++}(1232)K^-$	$F_1$	$0.17 \pm 0.07$
	$\phi_{F_1}$	$4.98 \pm 0.41$
	$F_2$	$0.38 \pm 0.13$
	$\phi_{F_2}$	$4.88 \pm 0.40$
$\Lambda^*(1520)\pi^+$	$H_1$	$0.18 \pm 0.09$
	$\phi_{H_1}$	$5.93 \pm 0.52$
	$H_2$	$0.20 \pm 0.07$
	$\phi_{H_2}$	$-0.06 \pm 0.55$
Nonresonant	$N_{++}$	$0.46 \pm 0.26$
	$\phi_{N_{++}}$	$3.48 \pm 0.54$
	$N_{+-}$	1.00
	$\phi_{N_{+-}}$	0.00
	$N_{-+}$	$0.18 \pm 0.15$
	$\phi_{N_{-+}}$	$0.75 \pm 0.71$
	$N_{--}$	$0.94 \pm 0.45$
	$\phi_{N_{--}}$	$1.13 \pm 0.36$
	Polarization [ $0 < p_T^2 < 0.70 \text{ GeV}/c^2$ ]	$\mathbf{P}_{\Lambda_c,1}$
Polarization [ $0.70 < p_T^2 < 1.24 \text{ GeV}/c^2$ ]	$\mathbf{P}_{\Lambda_c,2}$	$-0.22 \pm 0.25$
Polarization [ $1.24 < p_T^2 < 5.20 \text{ GeV}/c^2$ ]	$\mathbf{P}_{\Lambda_c,3}$	$-0.67 \pm 0.15$
# Signal Events	$N_S$	$946 \pm 38$
# Background Events	$N_B$	$1324 \pm 43$
Background Quadratic Term	$b_q$	$-0.98 \pm 10.51$
Background Linear Term	$b_l$	$1.34 \pm 0.48$
$\Lambda_c$ Mass ( $\text{GeV}/c^2$ )	$m_0$	$2.29 \pm 0.00$
$\Lambda_c$ Width ( $\text{MeV}/c^2$ )	$\sigma_a$	$20.1 \pm 4.8$
	$\sigma_b$	$9.3 \pm 0.6$

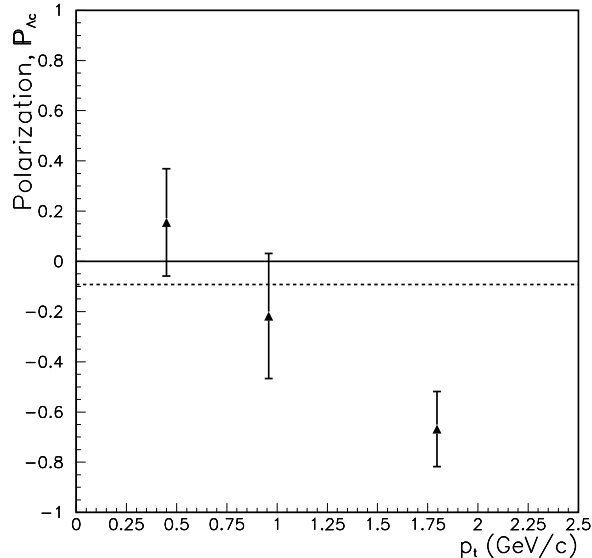


Fig. 3. The polarization of the  $\Lambda_c$  as a function of the  $\Lambda_c$ 's transverse momentum. The vertical bars represent the error as found by MINUIT. They are placed at the average  $p_T^2$  value for that region. Bin sizes are as in Table 7. The dotted line is the value of the polarization integrated over  $p_T^2$ .

agreement of the one-dimensional projections of the model and the data is 1.06. Although this agreement is reasonable, there are discrepancies, especially in the pK-mass-squared distribution. A model with a spin  $\frac{1}{2}^-$  resonance decaying to pK and having a mass of  $1.556 \pm 0.019$  GeV/ $c^2$  and width of  $279 \pm 74$  MeV/ $c^2$  reduces the overall  $\chi^2$  of the fit. However, there is no known resonance with this description. Trying another fit model, we find some evidence for an upper tail of the  $\Lambda(1405)(\rightarrow pK)$  [15]. Similarly, an improvement may be obtained by inclusion of nonresonant contributions beyond s-wave. In the case of each of these other models, the data are not sufficient to provide compelling evidence and/or to give significant measurements of the required additional parameters for the models. Figure 5 shows the one-dimensional projections of the model's resonant and nonresonant components, background, and total fit.

We calculate the fit fraction associated with each decay using Equation 6. A fit fraction  $F_i$  is the fraction of our signal described by decay via the  $i^{th}$  contribution and is the ratio of the magnitude squared of the amplitude term describing this contribution and the complete probability of the decay:

$$F_i = \frac{\int \sum_{m,\lambda_p} |B_i(m_i)\alpha_{i,m,\lambda_p}|^2 d\vec{x}}{\int \sum_{m,\lambda_p} |\sum_j B_j(m_j)\alpha_{j,m,\lambda_p}|^2 d\vec{x}} \quad (6)$$

using the notation of Equation 1 where  $\int d\vec{x}$  implies integrating over the decay phase space.

The major systematic errors on the fit fractions come from uncertainties in

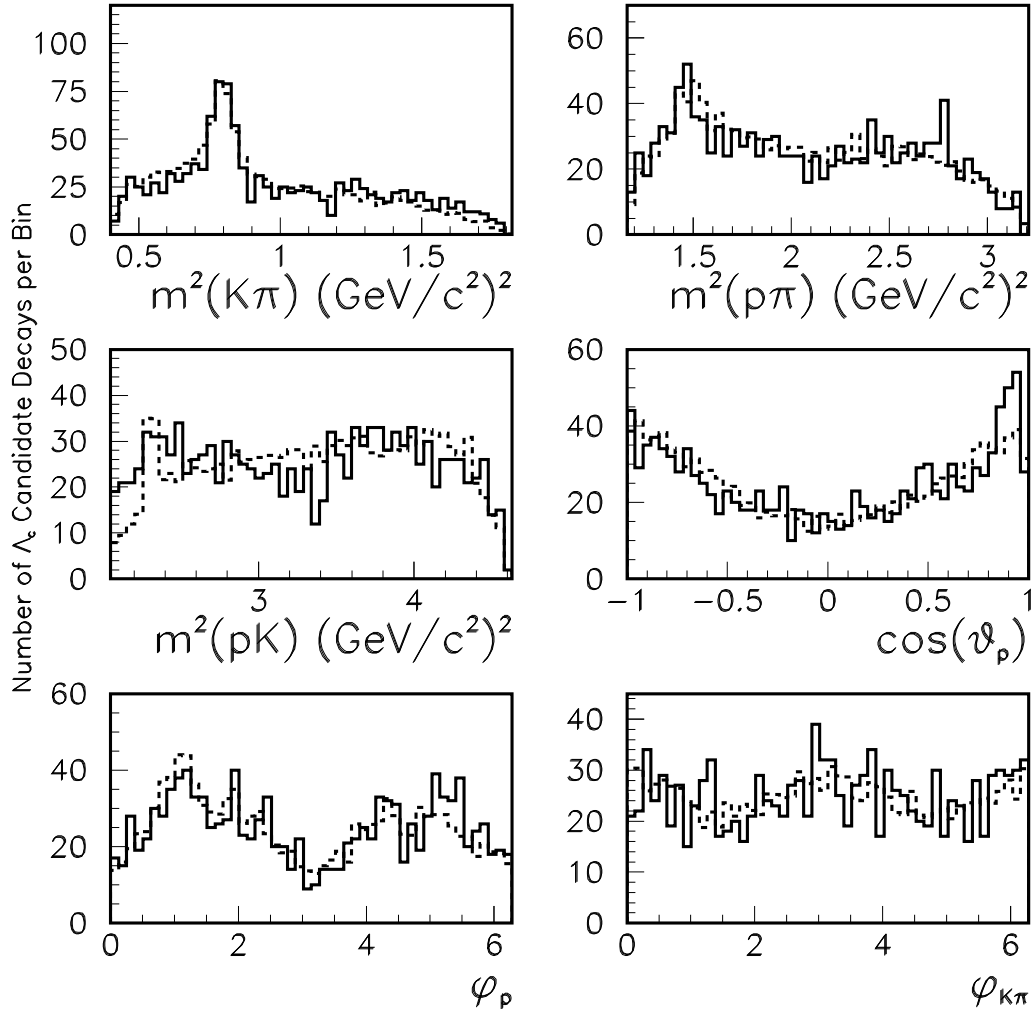


Fig. 4. Projections of the data within the  $m_{pK\pi}$  range of  $(2.265 - 2.315 \text{ GeV}/c^2)$  and overall fit superimposed. The data are shown as a solid histogram and the fits as dashed lines. There are 50 bins in each plot.

the performance of our Čerenkov counters and drift chambers, in the MC model for the production of  $\Lambda_c^+$  baryons, and in the adjustment of the  $K$ -nearest-neighbors model to the one-dimensional projections. In each case, a different model of acceptance is studied and the change in the central values of parameters is taken to be an estimate of the systematic error. Table 8 lists the uncertainties in the fit fractions due to these various sources.

The fit fractions for  $\Lambda_c^+ \rightarrow pK^-\pi^+$  are listed in Table 9, along with the statistical (first) and systematic (second) uncertainties. A check of these results is made by fitting the data assuming a single, average polarization. The resulting polarization is  $\mathbf{P}_{\Lambda_c} = -0.09 \pm 0.14$  (shown as the dotted line in Figure 3). The component fit fractions do not change significantly.

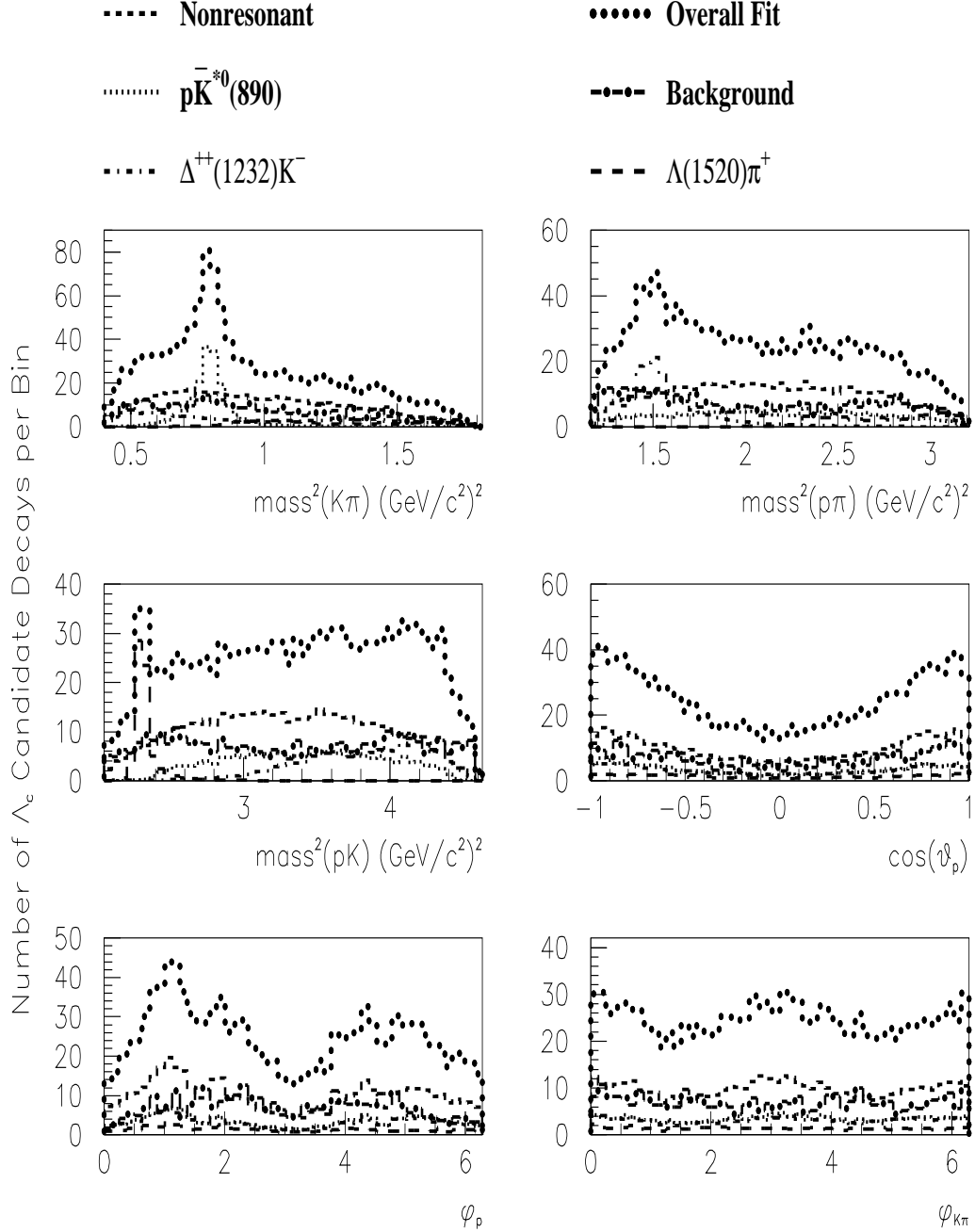


Fig. 5. Projections of the overall fit components scaled to match the number of data events within the  $m(pK\pi)$  range of  $(2.265 - 2.315 \text{ GeV}/c^2)$ . There are 50 bins in each plot.

Table 8

The systematic errors on fit fractions.

Mode	Drift	Čerenkov	Acceptance	Production	Combined
	Chamber (%)	Counter (%)	Adjust (%)	Model (%)	Error (%)
$p\bar{K}^{*0}(890)$	1.7	0.6	0.3	0.0	1.8
$\Delta^{++}(1232)K^-$	2.5	1.2	0.7	0.1	2.9
$\Lambda(1520)\pi^+$	0.9	0.5	0.4	0.1	1.1
Nonresonant	3.2	1.1	0.9	0.1	3.5

Table 9

The fit fractions for  $\Lambda_c^+ \rightarrow pK^-\pi^+$  with statistical and systematic errors from the final fit.

Mode	Fit Fraction (%)
$p\bar{K}^{*0}(890)$	$19.5 \pm 2.6 \pm 1.8$
$\Delta^{++}(1232)K^-$	$18.0 \pm 2.9 \pm 2.9$
$\Lambda(1520)\pi^+$	$7.7 \pm 1.8 \pm 1.1$
Nonresonant	$54.8 \pm 5.5 \pm 3.5$

Our results are compared to other published results in Table 10. The components in this decay do not demonstrate significant interference. This is most easily demonstrated by the fact that the fit fractions in Table 9 sum to near unity. Although we have better statistics than previous measurements, the uncertainties are comparable due to our more general fit.

Table 10

 $\Lambda_c^+$  branching ratios relative to the inclusive  $\Lambda_c^+ \rightarrow pK^-\pi^+$  branching fraction. The NA32 and ISR values were calculated from one-dimensional projections only.

Mode	E791	NA32[16]	ISR[17]
$p\bar{K}^{*0}(890)$	$0.29 \pm 0.04 \pm 0.03$	$0.35^{+0.06}_{-0.07} \pm 0.03$	$0.42 \pm 0.24$
$\Delta^{++}(1232)K^-$	$0.18 \pm 0.03 \pm 0.03$	$0.12^{+0.04}_{-0.05} \pm 0.05$	$0.40 \pm 0.17$
$\Lambda(1520)\pi$	$0.15 \pm 0.04 \pm 0.02$	$0.09^{+0.04}_{-0.03} \pm 0.02$	
Nonresonant	$0.55 \pm 0.06 \pm 0.04$	$0.56^{+0.07}_{-0.09} \pm 0.05$	

## 5 Discussion and Conclusions

Significant resonant and non-resonant branching fractions are found in this analysis of  $946 \pm 38$   $\Lambda_c^+ \rightarrow pK^-\pi^+$  signal events, the largest sample ever

analyzed. The size of the sample allows for inclusion of relative phases of the various contributions and a full accounting of spin and production polarization for the first time in such an analysis. The  $\Delta(1232)^{++}K^-$  and  $\Lambda(1520)\pi^+$  decay modes are seen as statistically significant contributions for the first time, even when uncertainties associated with phases and other variables are included. The observation of a substantial  $\Delta^{++}K^-$  component provides strong evidence for the W-exchange amplitude in charm baryon decays. The observed components of the  $\Lambda_c^+ \rightarrow pK^-\pi^+$  decay do not interfere significantly. Finally, we find no evidence for either  $\Lambda(1600)\pi^+$  or  $\Sigma(1660)\pi^+$  in the data.

In spite of the improvements in the  $\Lambda_c^+ \rightarrow pK^-\pi^+$  results coming from inclusion of the newly observed contributions, there remains poor agreement between the fit and the data in the pK-mass-squared projection. Additional data from new experiments are needed in order to conclusively demonstrate additional resonances (or their tails).

We find evidence for an increasingly negative polarization of the  $\Lambda_c$  baryons as a function of  $p_T^2$ , in agreement with a recent model[1] and, for large negative decay asymmetry, the measurement of Ref. [2]. As suggested by the authors of the model, the assumption of T-invariance leads to further constraints on resonant phases. Again, our data are consistent with these constraints but additional data from new experiments are needed for a stringent test of CP violation.

## 6 Acknowledgements

It is a pleasure to acknowledge useful conversations with William Dunwoodie, Gary Goldstein, and Fred Myhrer. We gratefully acknowledge the staffs of Fermilab and of all the participating institutions. This research was supported by the Brazilian Conselho Nacional de Desenvolvimento Científico e Tecnológico, the Mexican Consejo Nacional de Ciencia y Tecnología, the Israeli Academy of Sciences and Humanities, the U.S. Department of Energy, the U.S.-Israel Binational Science Foundation, and the U.S. National Science Foundation. Fermilab is operated by the Universities Research Association, Inc., under contract with the United States Department of Energy.

## References

- [1] W. G. D. Dharmaratna and G. R. Goldstein, Phys. Rev. D53 (1996) 1073. See also hep-ph/9907573 by Gary R. Goldstein.

- [2] M. Jezabek, K. Rybicki, and R. Rylko, Phys. Lett. B286 (1992) 175. Note that this reference has a normal to the production plane opposite to the convention adopted by their Ref. [10], by us and by Ref. [1].
- [3] Particle Data Group, “Review of Particle Physics”, Eur. Phys. J. C3 (1998) 1 and references therein.
- [4] E687 Collaboration, P. L. Frabetti et al., Phys. Lett. B331 (1994) 217.
- [5] D. Aston et al., Nucl. Phys. B296 (1988) 493.
- [6] R. Koch and E. Pietarinen, Nucl. Phys. A336 (1980) 331.
- [7] M. B. Watson, M. Ferro-Luzzi, and R. D. Tripp, Phys. Rev. 131 (1963) 2248.
- [8] H. Pilkuhn, Relativistic Particle Physics (Springer-Verlag, New York, 1979).
- [9] M. Jacob and G. C. Wick, Annals Phys. 7 (1959) 404. See also M. Perl, High Energy Hadron Physics (John Wiley & Sons, Inc., New York, 1974) and H. Pilkuhn, The Interactions of Hadrons (John Wiley & Sons, Inc., New York, 1967).
- [10] J. G. Körner and H. W. Siebert, Ann. Rev. Nucl. Part. Sci. 41 (1991) 511.
- [11] E791 Collaboration, E. M. Aitala et al., Phys. Lett. B371 (1996) 157 and references therein.
- [12] E791 Collaboration, E. M. Aitala et al., EPJdirect C4 (1999) 1.
- [13] C. M. Bishop, Neural Networks for Pattern Recognition (Clarendon Press, Oxford, 1995), p.55.
- [14] F. James and M. Goossens, “MINUIT Function Minimization and Error Analysis Reference Manual”, CERN Program Library Long Writeup D506, 1992.
- [15] R. Dalitz in [3], p. 676.
- [16] ACCMOR Collaboration, A. Bozek et al., Phys. Lett. B312 (1993) 247.
- [17] Split Field Magnet Collaboration, M. Basile et al., Nuovo Cim. 62A (1981) 14.